

Self-Guided Growth of Electronically Decoupled C₆₀ on Graphene on Rh(110)

Haojie Guo,* Antonio J. Martínez-Galera,* and José M. Gómez-Rodríguez

The authors report on the behavior of C₆₀ molecules adsorbed on graphene (Gr) monolayers grown on Rh(110), studied by means of scanning tunneling microscopy and spectroscopy under ultra-high vacuum conditions. Fullerene molecules form a well-ordered close packed hexagonal layout with an intermolecular distance of ≈ 1 nm. As demonstrated from the experimental data, the molecular packing direction of C₆₀ is locally close to being aligned with the quasi-1D moiré patterns formed by graphene on the metal support. Moreover, for certain orientations of graphene on Rh(110), the underlying moiré pattern appears superimposed on the molecular assembly. However, the analysis of the highest occupied molecular orbital and the lowest unoccupied molecular orbital structures and the differential conductance curves of C₆₀ on Gr/Rh(110) suggest a weak molecule–substrate interaction, similar to other 2D material/metal interfaces. All these observations can imply that the moiré structures of Gr/Rh(110) play a central role in the arrangement of C₆₀, but without modifying its electronic properties, which makes this Gr/Rh(110) system a singular platform for C₆₀ adsorption. Complementarily, the structural properties of multilayer growth of C₆₀ on Gr/Rh(110) are also investigated.

1. Introduction

With the rise of graphene (Gr) and related 2D materials, the surfaces of most of these one-atom thick elements have become a new paradigm for fundamental studies on molecular adsorption.^[1,2] Due to the 2D nature of these materials, their properties can be easily tuned by their interaction with other elements placed in their local vicinity, as is, for instance, the case of a supporting substrate.^[2–4] This fact has allowed obtaining complex interfaces, with tailored properties, comprising 2D materials. Interesting examples are the graphene–metal interfaces, which are characterized by periodic structural and chemical modulations, frequently known as moiré patterns.^[2–5] As a result, these superstructures offer an ample variety of chemical environments for molecular adsorption, opening the door to achieving a wide richness of different adsorption configurations, which will be also dependent on the specific features of the

adsorbate. Moreover, the diversity of potential adsorption configurations can be enlarged given the fact that the periodicity and the symmetry of the moiré pattern, as well as the interfacial chemistry, can be tuned by the election of the composition and the symmetry of the atomic lattice of the support.^[2–4,6]

C₆₀ is an archetype semiconducting organic molecule, whose intermolecular interaction is governed mainly through van der Waals forces. This molecule has recently reattracted an enormous interest due to its prospect to act as a basic building block that could be integrated with different 2D materials, giving rise to the formation of C₆₀/2D materials hybrid heterostructures.^[7–10] Such organic–inorganic heterostructure has been proposed to be highly promising in future technological applications because it may show different functionalities depending on the chosen 2D material.^[8,11] Therefore, a detailed characterization of the interfaces of C₆₀ molecules with the underlying 2D material would be a fundamental issue regarding the rational design of the upcoming nanodevices.

The C₆₀ molecule has previously been investigated on various 2D material/metal substrates, such as Gr/Ru(0001),^[12,13] Gr/SiC(0001),^[14,15] Gr/Cu(111),^[16] and also on the analog hexagonal boron nitride (h-BN)/metal systems.^[17–20] In some of these cases, the spatial and chemical modulation arising due to the moiré patterns have been proven to influence the assembly and structuring of the molecules on the surface, which, in turn,

H. Guo, J. M. Gómez-Rodríguez
 Departamento de Física de la Materia Condensada
 Universidad Autónoma de Madrid
 Madrid E-28049, Spain
 E-mail: haojie.guo@uam.es

A. J. Martínez-Galera
 Departamento de Física de Materiales
 Universidad Autónoma de Madrid
 Madrid E-28049, Spain
 E-mail: antonio.galera@uam.es

A. J. Martínez-Galera, J. M. Gómez-Rodríguez
 Instituto Nicolás Cabrera
 Universidad Autónoma de Madrid
 Madrid E-28049, Spain

J. M. Gómez-Rodríguez
 Condensed Matter Physics Center (IFIMAC)
 Universidad Autónoma de Madrid
 Madrid E-28049, Spain

 The ORCID identification number(s) for the author(s) of this article can be found under <https://doi.org/10.1002/admi.202202483>.

© 2023 The Authors. Advanced Materials Interfaces published by Wiley-VCH GmbH. This is an open access article under the terms of the Creative Commons Attribution License, which permits use, distribution and reproduction in any medium, provided the original work is properly cited.

DOI: 10.1002/admi.202202483

could affect the electronic properties of the molecular adsorbates. In contrast, for some others, the effect of the moiré patterns is negligible, and the molecule–substrate interaction is very weak. Nonetheless, all these studies have been mainly focused on 2D material/metal systems showing hexagonal symmetric moiré patterns, while the behavior of C_{60} on interfaces showing quasi-1D fringe-like moiré patterns is still little explored. Among the different 2D material/metal systems that could give place to the appearance of quasi-1D moiré patterns, the Gr/Rh(110) substrate is singular due to its properties. Previous results have shown that, despite the low apparent corrugation of the quasi-1D moiré patterns measured by scanning tunneling microscope (STM),^[6] on the surface coexist at least two distinguished chemical bonding-state of C atoms as demonstrated by X-ray photoelectron spectroscopy (XPS) data.^[21] Hence, it is highly interesting to understand how the low-corrugated but chemically modulated quasi-1D moiré patterns may affect the structural and electronic properties of C_{60} fullerene.

In this work, the behavior of C_{60} on single layers of graphene grown on Rh(110) has been studied by STM and scanning tunneling spectroscopy (STS) measurements under ultra-high vacuum (UHV) conditions. As inferred from the experimental data, while the quasi-1D moiré patterns of Gr/Rh(110) substrate drive the growth of C_{60} molecules, they do not influence, at least to a significant extent, the electronic features of this adsorbate. Thus, this case is at variance with the available literature on the adsorption of this archetypical molecule, suggesting an intermediate molecule–substrate interaction strength, which adds a new picture to the behavior of C_{60} on 2D materials/metals interfaces.

2. Results and Discussion

Figure 1a shows a STM topographic image acquired after C_{60} deposition, in the submonolayer regime, on a single-atom-thick graphene sheet, previously grown on a single crystal Rh(110) substrate. As can be seen, C_{60} molecules form a long-range ordered structure, with a high degree of crystalline quality, except for the very few defects indicated by the black circles. A magnified STM image on one of those molecular islands is displayed in **Figure 1b**, where a close-packed hexagonal arrangement of C_{60} can be observed. The lateral separation between adjacent C_{60} units is measured to be $a = 1.0 \pm 0.1$ nm. **Figure 1c,d** shows two STM topographic images, where the continued growth of C_{60} molecules across single and double atomic steps of Rh(110) beneath graphene is proved, as is evidenced by the height profiles depicted in **Figure 1e**.

The growth of C_{60} has been explored widely before on noble metals,^[22–29] graphene,^[12,14–16,30] as well as on h-BN.^[17–20] On all these surfaces, the formation of close-packed hexagonal layouts of C_{60} molecules was reported, which agrees with the experimental data shown in **Figure 1a,b**. As in all these cases, the formation of the periodic molecular assembly suggests a predominant role of the cohesive molecule–molecule interaction, which is reinforced by the fact that single isolated molecules were not observed at room temperature (RT), even at very low coverages. The lateral separation of ≈ 1 nm between neighbor C_{60} units is very close to those values reported on

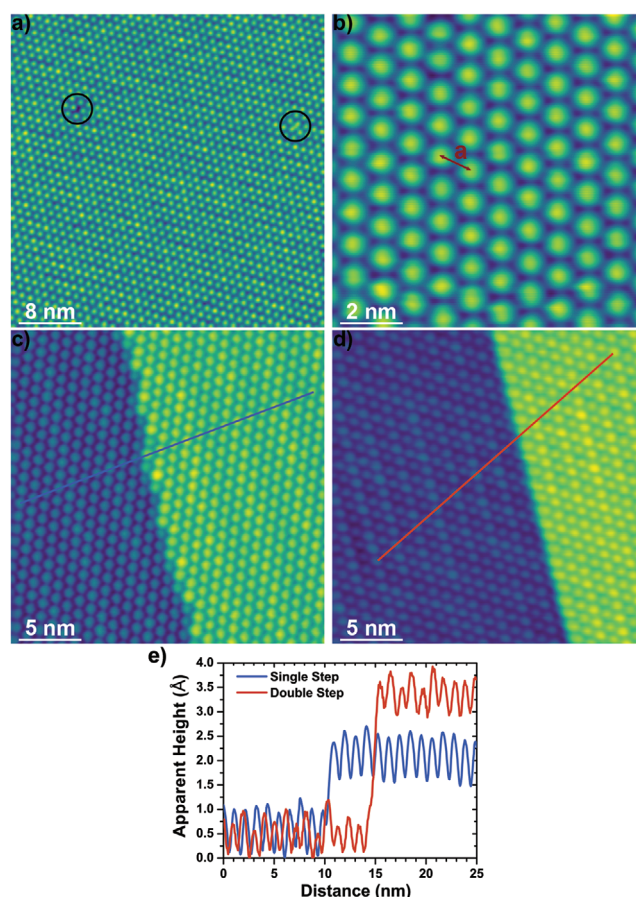


Figure 1. Structural properties of the C_{60} monolayer grown on Gr/Rh(110). a) Overall STM image displaying the high quality packing of C_{60} molecules deposited on Gr/Rh(110), with only very few defects indicated by the black circles. b) Magnified STM image of a C_{60} island on Gr/Rh(110), revealing a closed-packed hexagonal arrangement, with a lateral separation $a = 1.0 \pm 0.1$ nm. c,d) STM images showing the smooth and uninterrupted growth of C_{60} monolayers across single and double atomic steps of Rh(110), as can be inferred from the height profile depicted in (e). Tunneling parameters: $V_s = 1.5$ V; $I_t = 0.1$ nA; 40×40 nm² (a). $V_s = 1.8$ V; $I_t = 0.25$ nA; 10×10 nm² (b). $V_s = 1.7$ V; $I_t = 0.1$ nA; 25×25 nm² (c). $V_s = 1.50$ V; $I_t = 0.2$ nA; 25×25 nm² (d).

Gr/SiC(0001),^[15] Gr/Cu(111),^[16] h-BN/Ni(111),^[19] or h-BN/Rh(110),^[20] where the C_{60} molecules form a (4×4) superstructure with respect to the graphene/h-BN lattices. However, in the present case, the influence of the underlying substrate goes a step beyond, and such commensurate molecular assembly can be discarded, as will be discussed later. The uninterrupted growth of C_{60} across atomic steps of Rh(110), as it is proved in **Figure 1c–e**, could be understood in terms of the “carpet” like behavior of graphene on most metals, which means that the graphene sheet is not truncated by the underlying metal atomic steps.^[31–33] Therefore, the molecular ordering of C_{60} molecules is not affected by the highly reactive undercoordinated atoms placed at the metal substrate steps.

To gain insight into the possible influence of the underlying Gr/Rh(110) substrate on the self-assembly of C_{60} , measurements displaying simultaneously the molecular packing direction and the moiré patterns of the Gr/Rh(110) substrate have

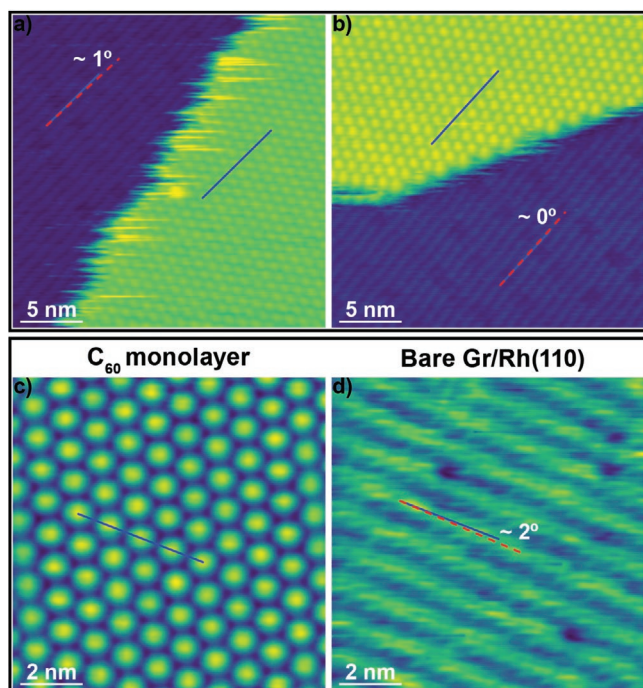


Figure 2. C_{60} molecular packing orientation with respect to the substrate. a,b) STM topographic images showing simultaneously a C_{60} molecular island and the Gr/Rh(110) substrate nearby. c) STM image of the molecular arrangement of C_{60} . d) STM image of the Gr/Rh(110) surface in the close vicinity of the molecular island shown in (c). In all the images, the characteristic stripe-like moiré pattern of Gr/Rh(110) and one of the high symmetry packing directions of C_{60} is highlighted by the dashed red and solid blue lines, respectively. Tunneling parameters: $V_s = -2.1$ V; $I_t = 50$ pA; 25×25 nm² (a). $V_s = -2.1$ V; $I_t = 0.1$ nA; 25×25 nm² (b). $V_s = 0.8$ V; $I_t = 0.5$ nA; 10×10 nm² (c). $V_s = 0.9$ V; $I_t = 0.2$ nA; 10×10 nm² (d).

been carried out. **Figure 2a,b** shows two STM images, acquired in different sample regions, that illustrate this strategy. As can be noticed, the molecular packing direction is almost aligned with respect to the moiré fringes direction of the Gr/Rh(110) system. As this kind of measurement is challenging to be executed, to back up the observed data shown in **Figure 2a,b**, a more extensive analysis has been performed by following a different approach (see **Figure 2c,d**). This consists of measuring, separately, the C_{60} molecular island (**Figure 2c**) and, immediately, the bare Gr/Rh(110) area nearby (**Figure 2d**). A similar conclusion can be reached, within the STM imaging uncertainty, by contrasting both images: the molecular packing and the Gr/Rh(110) moiré direction are close to being parallel.

All these observations recollected from **Figure 2** point toward a major role played by the 1D moiré pattern of Gr/Rh(110) on the self-assembly of C_{60} molecules because the molecular islands are forced to adopt an orientation such that one of the high-symmetry packing directions is parallel or nearly parallel with respect to the underlying stripes. Here, it should be mentioned that for rotational domains, in which graphene is aligned, or nearly aligned, with the [001] direction of Rh, the moiré stripes are aligned, or nearly aligned, with respect to the atomic lattice of graphene.^[21] However, the near alignment of one of the high symmetry directions of the C_{60} assembly with the moiré stripes has been found over different rotational variants

of the graphene/Rh(110) system (see **Figure 2a–c**). It suggests a major influence of the moiré stripes over the graphene lattice on the molecular arrangement. The influence of the moiré modulation, formed at the interface between 2D materials and metal surfaces, on the self-assembly of C_{60} molecules has already been documented before on Gr/Ru(0001),^[12,13] h-BN/Rh(111),^[17] or h-BN/Pd(110).^[18] In these cases, the moiré patterns have as a common feature, a strong corrugation. However, in other systems, which are characterized by exhibiting weak corrugations, such effect of the moiré patterns is negligible or undetectable like Gr/Cu(111)^[16] or h-BN/Rh(110).^[20] Interestingly, despite the moiré corrugation of Gr/Rh(110) being relatively low (≈ 0.3 Å), they are able to guide the C_{60} assembly.

Nevertheless, it is noteworthy to mention that deviation angles up to 5° have been measured, indicating that this apparent alignment between the molecular islands and the moiré patterns is not a global tendency, but more likely a local phenomenon. Such an idea could be rationalized in terms of two possible contributions: a stronger intermolecular interaction between C_{60} units compared to that between the molecules and the underlying Gr/Rh(110) surfaces, and the incommensurability between the C_{60} hexagonal layout and the stripes-like moiré patterns of Gr/Rh(110). The cohesive intermolecular forces provoke the molecules to form close-packed hexagonal arrangements as the energetically most favored geometry. On the other hand, due to the symmetry mismatch between the hexagonal disposal of the molecules and the stripe-like geometry of the moiré patterns of Gr/Rh(110), it seems to be very difficult to establish a commensurate long-range superstructure despite that the periodicity of the Gr/Rh(110) moiré patterns (≈ 1 nm) is quite similar to the separation between neighbors C_{60} molecules. Indeed, this similarity in the periodicities could also be a plausible explanation for the self-guided growth, locally, of C_{60} molecules along the moiré patterns direction. Therefore, in light of the above discussion, the emergence of a (4×4) superstructure of C_{60} , proposed on some Gr/metals^[15,16] or h-BN/metals^[18,20] systems, is rather unlikely on Gr/Rh(110).

Another experimental evidence of the influence of the underlying substrate on C_{60} deposited on Gr/Rh(110) is the observation of a faint long-range modulation permeating some STM images of fullerene islands. This phenomenon is illustrated in **Figure 3**. Specifically, **Figure 3a,d** depicts two STM images of close-packed C_{60} molecules, where the superimposed modulation can be observed, as highlighted by the dashed arrows. **Figure 3b,e** depicts the same STM images shown in **Figures 3a** and **3d**, respectively, after removing, by applying a band-stop filtering process, part of the signal contribution coming from the C_{60} hexagonal arrangement, to enhance the visibility of the modulation. The corresponding Gr/Rh(110) surface measured in a region adjacent to each of those molecular islands displayed in **Figure 3a,d** are shown in **Figures 3c** and **3f**, respectively. As it can be noticed, the long-range modulation visualized through the C_{60} molecules can also be recognized in the images of bare Gr/Rh(110) substrate (compare the dashed black arrows), having in both cases the same direction and the same periodicity.

To fully address the observations from **Figure 3**, a comprehensive description of the structural properties of Gr/Rh(110) system should be given beforehand. As previously reported,^[21]

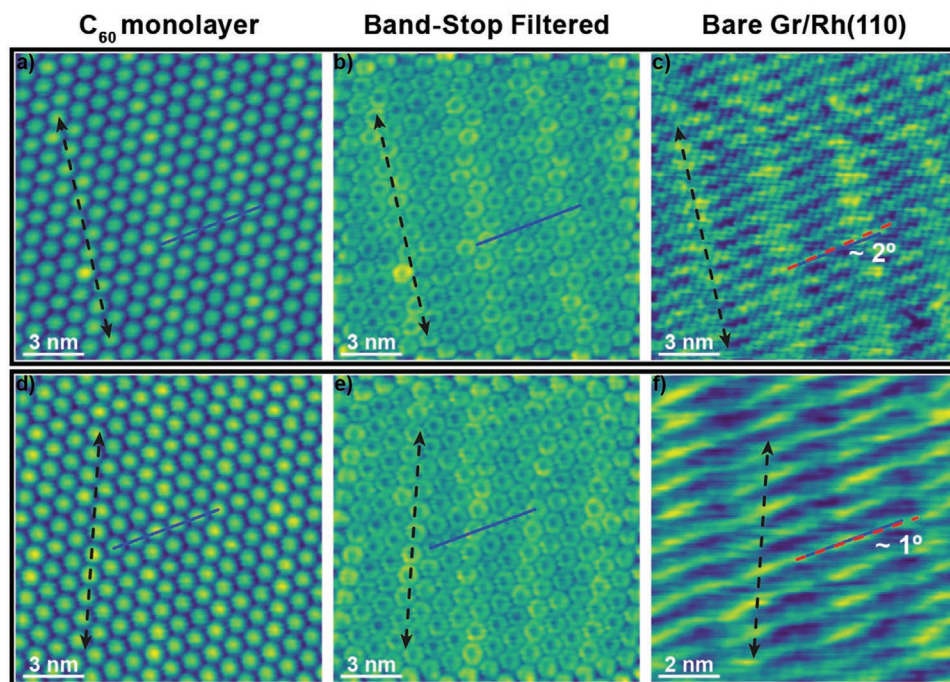


Figure 3. Effect of the substrate moiré pattern modulation on the C₆₀ molecular assembly. a,d) STM topographic images of C₆₀ molecular islands. b,e) Band-stop filtered STM images of (a) and (d), respectively, after removing part of the signal coming from the C₆₀ molecular assembly. c,f) Corresponding Gr/Rh(110) surface acquired in an adjacent region to the molecular islands of C₆₀ shown in (a) and (d). For all the images, the solid blue line, the dashed red line, and the dashed black arrow line represent the C₆₀ packing direction, and the fringes directions of the two sets of quasi-1D modulations of the moiré pattern of Gr/Rh(110), respectively. Tunneling parameters: V_s = 1.7 V; I_t = 0.1 nA; 15 × 15 nm² (a). V_s = 0.3 V; I_t = 0.6 nA; 15 × 15 nm² (c). V_s = 1.70 V; I_t = 0.1 nA; 15 × 15 nm² (d). V_s = 0.1 V; I_t = 0.6 nA; 10 × 10 nm² (f).

the high symmetry directions of the atomic arrangement of monolayers graphene grown on Rh(110) surfaces can adopt an infinity of possible orientations in the interval of (0°, ±10°) with respect to the [001] direction of the underneath Rh(110) surface. For some twist angles, mainly those close to 0°, the superposition of graphene monolayers on Rh(110) gives rise to the appearance of a single quasi-1D stripe-like moiré pattern on the surface. Notwithstanding, when the misalignment angle between graphene and Rh(110) significantly deviates from 0°, the as-formed moiré structures are composed of two interconnected sets of fringes. One of them has a periodicity akin to the moiré stripes formed for rotation angles close to 0°, whereas the other one possesses a larger periodicity, ranging from 2 to 6 nm. Bearing in mind these geometrical properties of the Gr/Rh(110) system, the stripe-like modulations observed in Figure 3c,f can be straightforwardly associated with the fingerprints of the double moiré patterns of Gr/Rh(110). It is interesting to note that, while the C₆₀ molecular packing direction is aligned, or nearly aligned, with the set of stripes of smaller periodicity, as discussed above in Figure 2, the latter is indetectable through the molecular assembly, opposite to what happens with the moiré fringes of larger separation (see Figure 3a,d). A possible explanation is that the low corrugation of the set of moiré stripes of smaller separation,^[6] along with the similarity between the separation of adjacent C₆₀ units and the periodicity of these moiré fringes may trigger that the latter are elusive to be imaged in STM through the molecular assembly. Likewise, the analog moiré stripes of the h-BN/Rh(110) system do

not appear imprinted on the molecular assemblies of C₆₀ and PTCDA.^[20,34]

To shed light on the electronic properties of C₆₀ on Gr/Rh(110), and to obtain more information about the interaction between molecule and substrate, frontiers molecular orbital imaging and differential conductance spectra have been carried out at a sample temperature of 40 K. Two different bias voltage-dependent intramolecular structures, acquired in the same sample area, are shown in Figure 4. It is interesting to note that all the C₆₀ units imaged in each image display identical submolecular features. In particular, a three-lobed shape structure is displayed in Figure 4a, while a two lobes structure, with one of them brighter than its counterpart, is depicted in Figure 4b. Likewise, Figure 4c depicts a *dI/dV* curve obtained by numerical differentiation of the average of ten individual *I/V* traces measured on top of a C₆₀ molecule. As can be noted from Figure 4c, the spectroscopy curve is characterized by two major peaks centered around −2.7 and +0.8 V.

C₆₀ is a spherical cage-like molecule comprised of electron-poor pentagon and electron-rich hexagon rings of carbon atoms. This complex bonding landscape is responsible for the existence of multiple potential adsorption configurations, and hence, of different possible orientations of the molecular cage over the substrate. As previously reported, C₆₀ molecules in a bulk crystal and also physisorbed on some surfaces adopt different cage orientations at RT,^[20,35–38] whereas, upon reducing the thermal energy, such randomness is reduced,^[35,39] and the molecules start to develop a single orientation at low

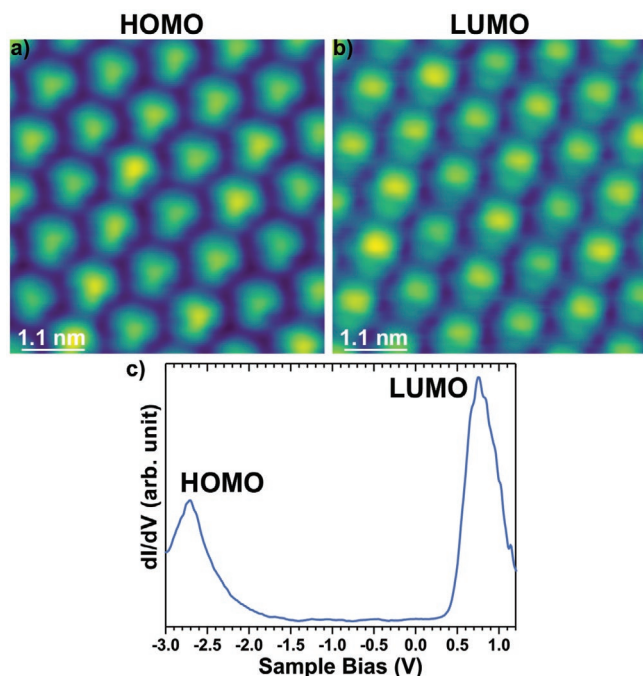


Figure 4. Electronic properties of C_{60} on Gr/Rh(110) at a sample temperature of 40 K. a,b) STM images showing, respectively, the highest occupied molecular orbital (HOMO) and lowest unoccupied molecular orbital (LUMO) structures of C_{60} . c) dI/dV spectra acquired from numerical differentiation of the average of ten $I-V$ curves measured on top of a C_{60} molecule. The two peaks centered at -2.7 and $+0.8$ V are ascribed to the HOMO and LUMO resonances, respectively. Tunneling parameters: $V_s = -2.7$ V; $I_t = 0.1$ nA; 5.5×5.5 nm 2 (a). $V_s = 0.9$ V; $I_t = 0.1$ nA; 5.5×5.5 nm 2 (b). Stabilization parameters: $V_s = -3$ V; $I_t = 0.1$ nA (c).

temperatures (<90 K).^[12,15,16,20,40,41] Thus, to eliminate the possible influence caused by the different orientations of individual C_{60} molecules at RT, their electronic properties have been studied at 40 K, where all the C_{60} molecules should have the same orientation.

Similar molecular orbital features as those exhibited in Figure 4a,b have been observed for C_{60} on Gr/Cu(111) at 1.2 K,^[16] where the authors attributed these intramolecular structures, respectively, to the highest occupied molecular orbital (HOMO) and the lowest unoccupied molecular orbital (LUMO) of C_{60} adsorbed on Gr/Cu(111). Even more, such HOMO and LUMO structures were ascribed to a specific cage orientation of C_{60} , in which there was a carbon atom at the topmost position of the molecular cage. In addition, this cage orientation had been reported to optimize the intermolecular forces between neighbors C_{60} units in the absence of a substrate.^[16,42] Consequently, the above description suggests that the orientational ordering at low temperatures in the present case of C_{60} on Gr/Rh(110) is still due to intermolecular forces despite the presence of the underlying Gr/Rh(110) surface. It implies further evidence of a very weak molecule–substrate interaction, which does not play an essential role in the cage orientation as it was also found on Gr/Cu(111). A similar conclusion can also be drawn from the dI/dV curve shown in Figure 4c. By contrasting the bias position of the peaks in the differential conductance curve with the voltages at which the HOMO and LUMO structures of Figure 4a,b

were obtained, the peaks centered at -2.7 V and 0.8 V could be associated with the HOMO and LUMO resonances of C_{60} molecules adsorbed on Gr/Rh(110). Hence, the energy gap of the C_{60} molecule, defined as the energy difference between the HOMO and LUMO peaks, has a value of ≈ 3.5 eV. This number is notably larger than for C_{60} adsorbed on metal surfaces such as Au(111),^[27,43] Ag(111),^[44] Ag(100),^[45] Cu(111),^[46] and Cu(100),^[47] where the C_{60} molecules undergo chemisorptive interaction with the underlying metal. However, the obtained experimental HOMO–LUMO gap, although smaller than that measured for bulk solid C_{60} (3.7 eV),^[48] is close to those measured on Gr/Cu(111) (3.4 eV),^[16] Gr/Ir(111) (3.4 eV),^[49] Gr/SiC(0001) (3.5 eV),^[14] or h-BN/Rh(110) (3.5 eV),^[20] for which weak physisorption has been reported. From these facts, it can be inferred that the C_{60} is electronically decoupled from Gr/Rh(110) substrate, with a lower interaction compared with metal surfaces.

Given the results presented here, it is valuable to draw an overall comparison of C_{60} adsorbed on Gr/metal and h-BN/metal systems, emphasizing the effect of the moiré patterns on the molecular arrangement and the electronic properties of the adsorbate. The highly corrugated moiré patterns of Gr/Ru(0001) constrain the C_{60} molecules to adsorb in specific sites of the moiré supercells, which, in turn, induces a shift in the LUMO state.^[13] In contrast, a decoupled system can be found for C_{60} on Gr/Cu(111), where the moiré patterns do not influence the adsorption behavior of fullerenes, and the study of the electronic properties reveals a very weak interaction with the substrate.^[16] The same conclusions for Gr/Cu(111) have also been extracted for C_{60} on h-BN/Rh(110).^[20] It is also interesting to point out that the moiré patterns of h-BN/Pd(110) and h-BN/Rh(111) act as templates that stamp their corrugation on the C_{60} overlayer. Nonetheless, the electronic properties of C_{60} on these surfaces have not been investigated yet. Thus, the C_{60} monolayer on Gr/Rh(110) reported in this work represents an intermediate case, where the electronic properties of C_{60} are demonstrated not to be significantly altered (comparable to Gr/Cu(111) or h-BN/Rh(110)) and, at the same time, there are some degrees of limitation in the adsorption and structuring of C_{60} due to the moiré patterns.

The growth of C_{60} thin films on Gr/Rh(110) has also been studied. Figure 5a displays a large scale STM image acquired after depositing a submonolayer coverage of C_{60} molecules on Gr/Rh(110). As it can be observed, bilayer and monolayer of C_{60} molecules coexist with the bare Gr/Rh(110) area. From the height profiles represented in the Figure 5b, obtained along the color lines indicated in Figure 5a,c, it can be deduced that both bilayer and trilayer have a similar apparent height, but are larger than the monolayer. Figure 5d displays an STM image measured along the boundary between monolayer and bilayer C_{60} molecules. Using the overlaid hexagonal lattice, the position of the molecules on the second layer has been determined to be centered over the threefold symmetry sites of the first layer. Likewise, within the STM error, differences in the lateral intermolecular spacing between the monolayer and bilayer have not been detected.

As it can be noticed from Figure 5a,c, the bilayer and trilayer molecules start to grow before the first layer is fully terminated, indicating that C_{60} thin film molecules follow a Stranski–Krastanov growth mode. Such behavior of C_{60} molecules on

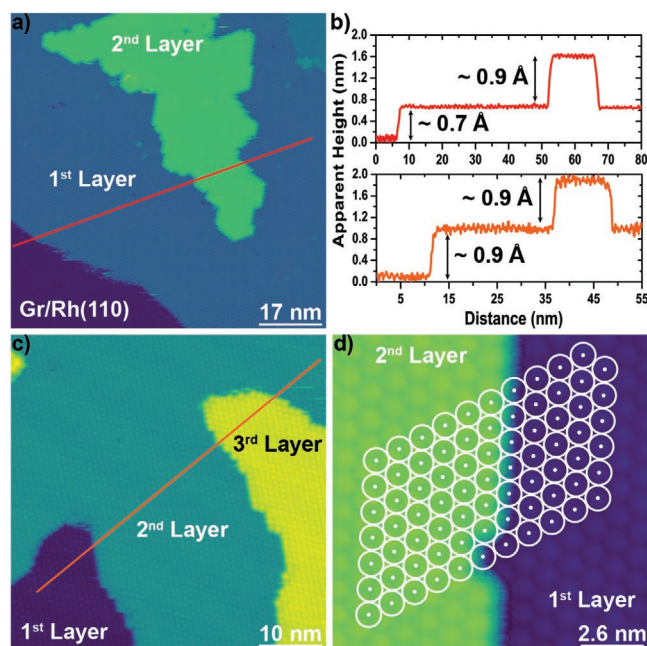


Figure 5. Multilayer growth of C_{60} on Gr/Rh(110). a) Large-scale STM image showing the early stages of multilayer growth of C_{60} on Gr/Rh(110) at RT. Bare substrate area coexists with first and second layer of C_{60} molecules. b) Apparent height profiles along the colored lines drawn in (a) and (c). c) STM topographic image illustrating a region where up to three C_{60} molecular layers are observed at the same time. d) Adsorption position of the second molecular layer with respect to the first layer. Tunneling parameters: $V_s = 1.65$ V; $I_t = 0.1$ nA; 85×85 nm² (a). $V_s = 1.5$ V; $I_t = 0.2$ nA; 50×50 nm² (c). $V_s = 1.65$ V; $I_t = 0.1$ nA; 13×13 nm² (d).

Gr/Rh(110) is akin to what happened on h-BN/Rh(110)^[20] but different from when they are deposited on metal surfaces,^[24,26] where they adopt a layer-by-layer growth mode (Frank-van der Merwe growth). In addition, as can be observed in Figure 5a (see also Figure S1a,b, Supporting Information), the molecular islands of multilayer C_{60} present a morphology that resembles to that of the multilayer growth of C_{60} on Gr/Ru(0001).^[13] Last, the determined stacking position of the bilayer with respect to the monolayer is in agreement also with previously reported results of bulk C_{60} ,^[35,39,41,50] where the molecules adopt a face-centered-cubic crystal lattice configuration. Moreover, such stacking configuration does not change for trilayer C_{60} with respect to the bilayer (see Figure S1c, Supporting Information), suggesting that this configuration should be conserved for even higher numbers of molecular layers.

3. Conclusion

In summary, the adsorption and thin film growth of C_{60} fullerene molecules on graphene grown on Rh(110) have been investigated via STM/STS under ultra-high vacuum. Self-assembled C_{60} molecules on Gr/Rh(110) form well-ordered and large molecular islands at RT, where the C_{60} units are arranged into a hexagonal assembly with a lateral separation of ≈ 1 nm. Besides, the C_{60} molecules experience, locally, the effects of the underlying moiré patterns of Gr/Rh(110). This is evidenced

by the fact that the molecular packing direction of C_{60} islands is aligned, or close to being parallel, with the quasi-1D moiré patterns of the substrate, as well as by the observation, in STM images, of the long-range modulation of one of the sets of moiré fringes overlaid to the C_{60} assembly. Nevertheless, despite the influence of the moiré patterns on the assembly of the molecules, the interaction of C_{60} with the Gr/Rh(110) surface is still weak and comparable with other Gr/metals and h-BN/metals systems as it is deduced from the analysis of the HOMO and LUMO structures and of differential conductance spectra, performed at 40 K. Last, multilayer growth of C_{60} on Gr/Rh(110) suggests a stacking behavior similar to the bulk C_{60} .

4. Experimental Section

The experiments were performed in a UHV system with a base pressure in the range of 1×10^{-10} Torr. This system consisted of two independent chambers, which allowed to keep separately sample preparation and characterization. The analysis chamber, that is, that employed for sample characterization, was set up with a custom-built variable temperature scanning tunneling microscope.^[51] Sample preparation started by cleaning the Rh(110) single-crystal through Ar⁺ sputtering at 1 kV, followed by annealing at 1220 K under oxygen atmosphere (2×10^{-6} Torr), and finishing with flash annealing in UHV at 1220 K. Gr monolayers were obtained using the chemical vapor deposition method (CVD) with ethylene (C_2H_4) as the precursor. The freshly cleaned Rh(110) surface, kept at 1170 K, was exposed to double cycles of 18 L and 26 L of ethylene at a partial pressure of 3×10^{-7} Torr to ensure that the whole metal surface was entirely covered by graphene. The structural quality of the Gr/Rh(110) surface was checked using STM before depositing the C_{60} molecules. They were sublimated from a home-built cell, loaded with high purity sources of solid C_{60} molecules, while keeping the Gr/Rh(110) surfaces at RT. The effusion cell was thoroughly outgassed before deposition of C_{60} on the Gr/Rh(110) surfaces. C_{60} coverages were referred to the molecular density of a closed layer.

All measurements were conducted at RT except when stated otherwise. STM data were registered in the constant current mode using tungsten tips, with the bias voltage applied to the sample. STM images were acquired and post-analyzed/processed using the commercially free WSxM software.^[52]

Supporting Information

Supporting Information is available from the Wiley Online Library or from the author.

Acknowledgements

Financial support from the Spanish Ministerio de Economía y Competitividad (MINECO) and Fondo Europeo de Desarrollo Regional (FEDER) under grant No. MAT2016-77852-C2-2-R, as well as, from the Spanish Ministerio de Ciencia e Innovación through the “María de Maetzu” program for units of excellence in R&D (grant No. CEX2018-000805-M) is gratefully acknowledged. A.J.M.-G. acknowledges funding by the Spanish MICINN through Project No. PID2020-116619GA-C22, as well as, from the Comunidad de Madrid and the Universidad Autónoma de Madrid under project SI3/PJI/2021-00500.

Conflict of Interest

The authors declare no conflict of interest.

Data Availability Statement

The data that support the findings of this study are available from the corresponding author upon reasonable request.

Keywords

2D materials, fullerene, molecular orbitals, molecular self-guided growth, STM/STS, symmetry mismatched substrates

Received: December 17, 2022

Revised: March 1, 2023

Published online: April 18, 2023

- [1] A. Kumar, K. Banerjee, P. Liljeroth, *Nanotechnology* **2017**, *28*, 082001.
- [2] W. Auwärter, *Surf. Sci. Rep.* **2019**, *74*, 1.
- [3] J. Wintterlin, M. L. Bocquet, *Surf. Sci.* **2009**, *603*, 1841.
- [4] M. Batzill, *Surf. Sci. Rep.* **2012**, *67*, 83.
- [5] C. Busse, P. Lazic, R. Djemour, J. Coraux, T. Gerber, N. Atodiressei, V. Caciuc, R. Brako, A. T. N'Diaye, S. Blugel, J. Zegenhagen, T. Michely, *Phys. Rev. Lett.* **2011**, *107*, 036101.
- [6] A. J. Martínez-Galera, J. M. Gomez-Rodriguez, *Nano Res.* **2018**, *11*, 4643.
- [7] D. Jariwala, T. J. Marks, M. C. Hersam, *Nat. Mater.* **2017**, *16*, 170.
- [8] M. Q. Chen, R. N. Guan, S. F. Yang, *Adv. Sci.* **2019**, *6*, 1800941.
- [9] K. Pei, T. Y. Zhai, *Cell Rep Phys Sci* **2020**, *1*, 100166.
- [10] X. M. Xu, Z. R. Lou, S. M. Cheng, P. C. Y. Chow, N. Koch, H. M. Cheng, *Chem* **2021**, *7*, 2989.
- [11] M. Gobbi, E. Orgiu, P. Samori, *Adv. Mater.* **2018**, *30*, 1706103.
- [12] G. Li, H. T. Zhou, L. D. Pan, Y. Zhang, J. H. Mao, Q. Zou, H. M. Guo, Y. L. Wang, S. X. Du, H. J. Gao, *Appl. Phys. Lett.* **2012**, *100*, 013304.
- [13] J. Lu, P. S. E. Yeo, Y. Zheng, Z. Y. Yang, Q. L. Bao, C. K. Gan, K. P. Loh, *ACS Nano* **2012**, *6*, 944.
- [14] J. Cho, J. Smerdon, L. Gao, O. Suzer, J. R. Guest, N. P. Guisinger, *Nano Lett.* **2012**, *12*, 3018.
- [15] M. Svec, P. Merino, Y. J. Dappe, C. Gonzalez, E. Abad, P. Jelinek, J. A. Martin-Gago, *Phys. Rev. B* **2012**, *86*, 121407(R).
- [16] M. Jung, D. Shin, S. D. Sohn, S. Y. Kwon, N. Park, H. J. Shin, *Nanoscale* **2014**, *6*, 11835.
- [17] M. Corso, W. Auwärter, M. Muntwiler, A. Tamai, T. Greber, J. Osterwalder, *Science* **2004**, *303*, 217.
- [18] M. Corso, T. Greber, J. Osterwalder, *Surf. Sci.* **2005**, *577*, L78.
- [19] M. Muntwiler, W. Auwärter, A. P. Seitsonen, J. Osterwalder, T. Greber, *Phys. Rev. B* **2005**, *71*, 121402(R).
- [20] H. Guo, A. J. Martínez-Galera, J. M. Gomez-Rodriguez, *Nanotechnology* **2021**, *32*, 025711.
- [21] A. J. Martínez-Galera, H. Guo, M. D. Jiménez-Sánchez, E. G. Michel, J. M. Gomez-Rodriguez, *Carbon* **2023**, *205*, 294.
- [22] Y. Zhang, X. P. Gao, M. J. Weaver, *J. Phys. Chem.* **1992**, *96*, 510.
- [23] E. I. Altman, R. J. Colton, *Phys. Rev. B* **1993**, *48*, 18244.
- [24] E. I. Altman, R. J. Colton, *Surf. Sci.* **1993**, *295*, 13.
- [25] T. Hashizume, K. Motai, X. D. Wang, H. Shinohara, Y. Saito, Y. Maruyama, K. Ohno, Y. Kawazoe, Y. Nishina, H. W. Pickering, Y. Kuk, T. Sakurai, *Phys. Rev. Lett.* **1993**, *71*, 2959.
- [26] K. Motai, T. Hashizume, H. Shinohara, Y. Saito, H. W. Pickering, Y. Nishina, T. S. T. Sakurai, *Jpn. J. Appl. Phys.* **1993**, *32*, L450.
- [27] C. Rogero, J. I. Pascual, J. Gomez-Herrero, A. M. Baro, *J. Chem. Phys.* **2002**, *116*, 832.
- [28] X. Zhang, F. Yin, R. E. Palmer, Q. Guo, *Surf. Sci.* **2008**, *602*, 885.
- [29] L. Tang, Y. C. Xie, Q. M. Guo, *J. Chem. Phys.* **2011**, *135*, 114702.
- [30] H. T. Zhou, J. H. Mao, G. Li, Y. L. Wang, X. L. Feng, S. X. Du, K. Mullen, H. J. Gao, *Appl. Phys. Lett.* **2011**, *99*, 153101.
- [31] J. Coraux, A. T. N'Diaye, C. Busse, T. Michely, *Nano Lett.* **2008**, *8*, 565.
- [32] P. W. Sutter, J. I. Flege, E. A. Sutter, *Nat. Mater.* **2008**, *7*, 406.
- [33] H. I. Rasool, E. B. Song, M. J. Allen, J. K. Wassei, R. B. Kaner, K. L. Wang, B. H. Weiller, J. K. Gimzewski, *Nano Lett.* **2011**, *11*, 251.
- [34] A. J. Martínez-Galera, J. M. Gomez-Rodriguez, *J. Phys. Chem. C* **2019**, *123*, 1866.
- [35] P. A. Heiney, J. E. Fischer, A. R. McGhie, W. J. Romanow, A. M. Denenstein, J. P. McCauley, A. B. Smith, D. E. Cox, *Phys. Rev. Lett.* **1991**, *66*, 2911.
- [36] R. D. Johnson, C. S. Yannoni, H. C. Dorn, J. R. Salem, D. S. Bethune, *Science* **1992**, *255*, 1235.
- [37] A. Goldoni, C. Cepek, S. Modesti, *Phys. Rev. B* **1996**, *54*, 2890.
- [38] S. I. Bozhko, S. A. Krasnikov, O. Lubben, B. E. Murphy, K. Radican, V. N. Semenov, H. C. Wu, B. Bulfin, I. V. Shvets, *Phys. Rev. B* **2011**, *84*, 195412.
- [39] P. A. Heiney, *J. Phys. Chem. Solids* **1992**, *53*, 1333.
- [40] W. I. F. David, R. M. Ibberson, J. C. Matthewman, K. Prassides, T. J. S. Dennis, J. P. Hare, H. W. Kroto, R. Taylor, D. R. M. Walton, *Nature* **1991**, *353*, 147.
- [41] W. I. F. David, R. M. Ibberson, T. J. S. Dennis, J. P. Hare, K. Prassides, *Europhys. Lett.* **1992**, *18*, 219.
- [42] C. L. Hsu, W. W. Pai, *Phys. Rev. B* **2003**, *68*, 245414.
- [43] X. H. Lu, M. Grobis, K. H. Khoo, S. G. Louie, M. F. Crommie, *Phys. Rev. B* **2004**, *70*, 115418.
- [44] R. Hesper, L. H. Tjeng, G. A. Sawatzky, *Europhys. Lett.* **1997**, *40*, 177.
- [45] X. H. Lu, M. Grobis, K. H. Khoo, S. G. Louie, M. F. Crommie, *Phys. Rev. Lett.* **2003**, *90*, 096802.
- [46] J. A. Larsson, S. D. Elliott, J. C. Greer, J. Repp, G. Meyer, R. Allenspach, *Phys. Rev. B* **2008**, *77*, 115434.
- [47] G. Schull, N. Neel, M. Becker, J. Kroger, R. Berndt, *New J. Phys.* **2008**, *10*, 065012.
- [48] T. R. Ohno, Y. Chen, S. E. Harvey, G. H. Kroll, J. H. Weaver, R. E. Haufler, R. E. Smalley, *Phys. Rev. B* **1991**, *44*, 13747.
- [49] X. M. Fei, X. Zhang, V. Lopez, G. Lu, H. J. Gao, L. Gao, *J. Phys. Chem. C* **2015**, *119*, 27550.
- [50] M. S. Dresselhaus, G. Dresselhaus, P. C. Eklund, *Science of Fullerenes and Carbon Nanotubes*, 8th ed, Academic Press, Cambridge, MA **1996**.
- [51] O. Custance, S. Brochard, I. Brihuega, E. Artacho, J. M. Soler, A. M. Baro, J. M. Gomez-Rodriguez, *Phys. Rev. B* **2003**, *67*, 235410.
- [52] I. Horcas, R. Fernandez, J. M. Gomez-Rodriguez, J. Colchero, J. Gomez-Herrero, A. M. Baro, *Rev. Sci. Instrum.* **2007**, *78*, 013705.